# 

Cite as: Appl. Phys. Lett. **114**, 253501 (2019); doi: 10.1063/1.5099957 Submitted: 13 April 2019 · Accepted: 1 June 2019 ·

Published Online: 24 June 2019







Samuel James Bader,<sup>1,a)</sup> © Reet Chaudhuri,<sup>2</sup> Martin F. Schubert,<sup>3</sup> Han Wui Then,<sup>4</sup> Huili Grace Xing,<sup>2,5,6</sup> ond Debdeep Jena<sup>2,5,6</sup>

#### **AFFILIATIONS**

- $^1$ School of Applied and Engineering Physics, Cornell University, Ithaca, New York 14853, USA
- <sup>2</sup>School of Electrical and Computer Engineering, Cornell University, Ithaca, New York 14853, USA
- <sup>3</sup>X Development LLC, 100 Mayfield Ave., Mountain View, California 94043, USA
- <sup>4</sup>Intel Corporation, 2501 NE Century Blvd., Hillsboro, Oregon 97124, USA

#### **ABSTRACT**

To make complementary GaN electronics a desirable technology, it is essential to understand the low mobility of 2D hole gases in III-Nitride heterostructures. This work derives both the acoustic and optical phonon spectra present in one of the most prominent p-channel heterostructures (the all-binary GaN/AlN stack) and computes the interactions of these spectra with the 2D hole gas, capturing the temperature dependence of its intrinsic mobility. Finally, the effects of strain on the electronic structure of the confined 2D hole gas are examined and a means is proposed to engineer the strain to improve the 2D hole mobility for enhanced p-channel device performance, with the goal of enabling wide-bandgap CMOS.

Published under license by AIP Publishing. https://doi.org/10.1063/1.5099957

Decades after the celebrated invention of Mg p-doping in Gallium Nitride (GaN) and the subsequent development of GaN-based light emitting diodes, the manipulation of holes in GaN remains a fundamental challenge. Consequently, despite the expected dominance of GaN High Electron Mobility Transistors (HEMTs) in the coming generation of power electronics<sup>2</sup> and communications systems,<sup>3</sup> there is no complementary p-channel device which can be readily integrated. This incompleteness restricts the possible circuit topologies and system designs achievable in GaN electronics but arises quite straightforwardly from the physics of the GaN valence band. These bands, both heavy and deep in energy, have proven difficult to contact with typical metal workfunctions,4 difficult to dope with high efficiency,5 and difficult to flow current through with high conductivity. Nonetheless, the commercial interest in generating complementary GaN-based circuits<sup>6</sup> and scientific interest in studying highly degenerate hole physics<sup>7</sup> have prompted great recent progress in p-channel devices.8

Of the various structures<sup>6,9–16</sup> which have been proposed as a platform for p-channel III-Nitride electronics, the single GaN/AlN heterojunction field-effect transistor has received recent attention for its high sheet conductance<sup>7</sup> and excellent device performance.<sup>8</sup> In this

structure, depicted in Fig. 1(a), the all-binary materials provide a straightforwardly repeatable growth with no possible parasitic electron channels, a tremendous hole-inducing polarization-charge for low sheet-resistance, and maximal bandgaps for extreme voltage-handling capability. Given the recent reports of temperature-dependent transport studies in this heterostructure<sup>7</sup> and recent first-principles suggestions of possible enhancements to hole mobility in bulk p-GaN, <sup>17</sup> this work presents a model to explain the measured mobility of the 2D hole gas (2DHG) at the GaN/AlN interface and evaluates the potential of strain-engineering approaches to alter the band structure in a favorable way. First, the valence band structure including confinement and multiband mixing effects is computed. Then, the spectra of both acoustic and optical phonons in the heterostructure are determined and the mobility limitation due to these mechanisms is derived. Finally, the effects of strain on the band structure and mobility are presented.

The multiband k.p (MBKP) approach, based on Burt Exact Envelope Function Theory, <sup>18,19</sup> describes the electronic states of heterostructures wherein multiple subbands may be intermixed by nonuniform potentials and material interfaces. MBKP has been extended to

 $<sup>^5</sup>$ Department of Materials Science and Engineering, Cornell University, Ithaca, New York 14853, USA

<sup>&</sup>lt;sup>6</sup>Kavli Institute at Cornell, Ithaca, New York 14853, USA

<sup>&</sup>lt;sup>a)</sup>sjb353@cornell.edu. URL: http://sambader.net

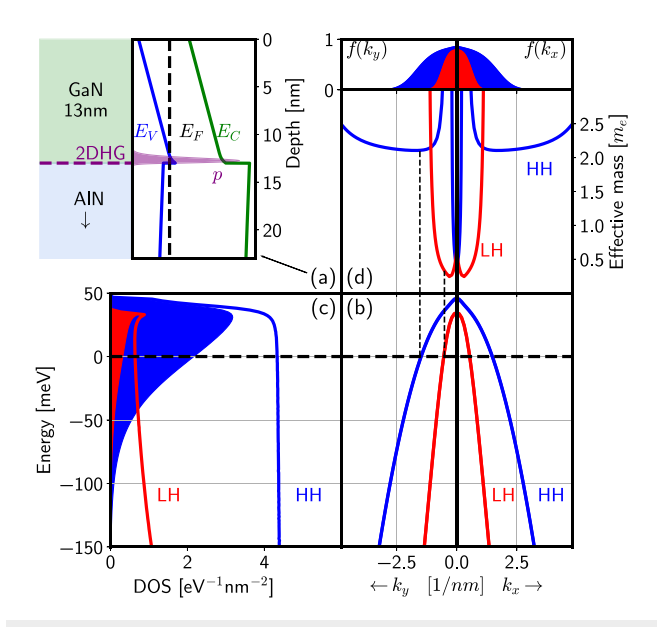


**FIG. 1.** (a) A 13 nm GaN layer on top of a thick AlN buffer induces a two-dimensional hole gas of density  $\sim$ 4.4  $\times$  10<sup>13</sup>/cm², which is confined at the interface by strong polarization fields. (b) The relevant bands are the first spin-degenerate HH subbandpair (blue) and LH subband-pair (red). (c) The DOS of the two bands is indicated by solid lines and the occupation of the bands by filled shapes. (d) The effective masses vs position in k-space, capped by the occupation probability as a function of k. The energy axes of (b) and (c) align, and the *k*-axes of (b) and (d) align. Dashed lines that show the effective masses near the Fermi energy are guides to the eye.

wurtzite heterostructures by various authors<sup>20,21</sup> and is available in certain commercial packages.<sup>22</sup> The PyNitride software package<sup>23</sup> employed here self-consistently<sup>24</sup> solves the 6 × 6 MBKP equation of the wurtzite valence band (see the supplementary material) simultaneously with the Poisson equation, accounting for the large fixed interface polarization charge. Figure 1(a) depicts a highly confined 2D hole gas at the GaN/AlN interface. The hole gas represents contributions mainly from the first quantized subband of both the heavy hole (HH) and light hole (LH) bands (including spin, this is four subbands). The transverse dispersion is shown in Fig. 1(b). By density, as clear from Fig. 1(c), the HH band dominates, though as shown in Fig. 1(d), the LH band has lighter in-plane mass near the Fermi energy, and so it contributes significantly to transport. To evaluate transport, we proceed to describe the phonons.

The Dielectric Continuum model<sup>25</sup> describes polar optical phonons (POPs) in arbitrary heterostructures. As POP scattering is the main limitation on electron mobility in quality GaN, numerous authors have invested significant theoretical effort into the elaboration of POP spectra in various wurtzite heterostructures.<sup>26–30</sup> A structure as simple as this, in fact, can be solved analytically. For a uniaxial crystal, the effect of polar optical phonons can be incorporated into two frequency ( $\omega$ ) dependent, directional dielectric functions,  $\varepsilon_{\perp}$  and  $\varepsilon_{\parallel}$ ,

$$\varepsilon_{\perp} = \varepsilon^{\infty} \frac{\omega_{LO\perp}^2 - \omega^2}{\omega_{TO\parallel}^2 - \omega^2} \quad \text{and} \quad \varepsilon_{\parallel} = \varepsilon^{\infty} \frac{\omega_{LO\parallel}^2 - \omega^2}{\omega_{TO\parallel}^2 - \omega^2}, \tag{1}$$

where those longitudinal ( $\omega_{LO}$ ) and transverse ( $\omega_{TO}$ ) POP frequencies and high-frequency dielectric constant  $\epsilon^{\infty}$  can be determined

experimentally for the materials in play (see tabulation in Komirenko et al.<sup>29</sup>). For a mode with in-plane wavevector q, the POP problem reduces to solving a frequency-dependent Poisson eigenvalue equation

$$\partial_z \epsilon_{\parallel} \partial_z \phi = q^2 \epsilon_{\perp} \phi \tag{2}$$

for the potential  $\phi$ . At every characteristic frequency appearing in Eq. (1), a dielectric constant changes sign, which changes the character of the involved modes (locally decaying vs oscillating). Altogether, there are three classes of modes depending on the energy range: (1) oscillating in GaN, decaying in AlN, (2) oscillating in AlN, decaying in GaN, and (3) decaying bidirectionally from a GaN/AlN interface. For each class, both transverse and longitudinal polarizations are possible. The spectrum and example modes are depicted in Fig. 2, and the solution is elaborated in the supplementary material.

The Elastic Continuum model<sup>25</sup> aptly describes acoustic phonons in arbitrary heterostructures. Given the centrality of "optical" phonons in electron-based devices, the literature on acoustic phonons in wurtzite heterostructures<sup>31–34</sup> is significantly less comprehensive. The basic approach is to link a continuum Newton's law with a material stress-strain relation

$$\rho \frac{\partial^2 u_i}{\partial t^2} = \frac{\partial T_{ij}}{\partial r_i}, \quad T_{ij} = c_{ijkl} \epsilon_{kl}, \tag{3}$$

where  $u_i$  is the local displacement vector,  $\rho$  is the density,  $T_{ij}$  is the stress tensor,  $c_{ijkl}$  is the stiffness tensor, and  $\epsilon_{ijkl}$  is the strain tensor  $\epsilon_{ij} = \frac{1}{2} \left( \partial_{r_j} u_i + \partial_{r_i} u_j \right)$ . Due to symmetry constraints on the stiffness tensor, the in-plane shear component is uncoupled ("Y" modes), while longitudinal and out-of-plane components constitute two coupled differential equations ("XZ" modes). These are solved by the Finite Element Method. For both types of modes, there are two characters

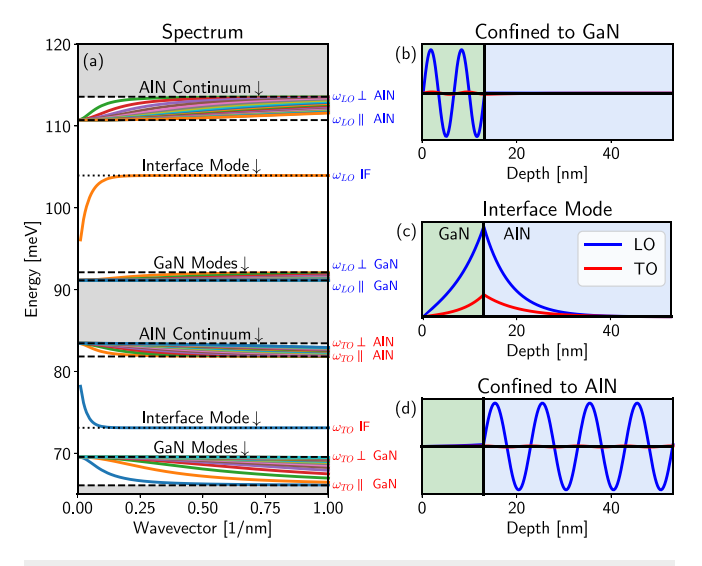


FIG. 2. Polar optical phonons. (a) Spectrum of the various extra-ordinary POP modes, with the character of each mode labeled. The bottom three bands (within red frequency labels) are predominantly transverse (TO), and the top three bands (within blue frequency labels) are predominantly longitudinal (LO). Examples of (b) modes confined to GaN, (c) to the interface, and (d) to AIN. For each, the potential of both possible polarizations is shown. As expected, the TO phonons contribute weaker potential

possible depending on the energy range. At energies above  $\hbar v_t q$ , where  $v_t$  is the relevant AlN sound velocity, modes are able to propagate in the AlN and are thus of a continuum sort. Below this energy, any modes which exist must decay into the AlN, so are GaN-confined modes. The spectrum and example modes are revealed in Fig. 3, and the solution methodology is elaborated in the supplementary material.

We now turn to the interactions of the phonons and carriers. First, both types of phonon modes are normalized<sup>25</sup> by the quantization condition  $\int d^3\vec{r} \, \rho(\vec{r}) |\vec{u}(r)|^2 = \frac{\hbar}{2\omega}$ . Once the oscillations are normalized, the Hamiltonian term for each mode can be generated. For optical phonons, this is just  $H_{pop}=-e\phi(r)$ . For acoustic phonons, the deformation potential  $H_{adp}=D(\epsilon)$  is a six-by-six matrix function of position: at each position, it recruits the valence deformation matrix of the local material and also the local strain from a given acoustic mode. There is also a (coherently combined) piezo term  $H_{pz} = -e\phi(r)$  where  $\phi$  is found<sup>32</sup> by solving the Poisson equation given the piezoelectric charge induced by the mode (see the supplementary material). Finally, to account for the low-temperature mobility, which is around 200 cm<sup>2</sup>/Vs in these structures to date, some extrinsic limitation must be included. The exact cause (e.g., interface roughness, dislocation, impurity, etc) is irrelevant to this study, since all these elastic mechanisms are temperature-independent and have similar dependence on effective masses. So the exact cause is not deduced here, but rather a generic scatterer with a constant scalar matrix element is applied to set the low-temperature mobility to 200 cm<sup>2</sup>/Vs. This matrix element is the only "tuning parameter."

To calculate the perturbed carrier distribution, we employ the linearized Boltzmann Transport Equation (LBTE)

$$\frac{q\vec{\mathcal{E}}}{\hbar} \cdot \nabla_{k} f_{m}^{0}(k) = \sum_{k'm'} R_{km}^{k'm'} f_{m}^{A}(k) - R_{k'm'}^{km} f_{m'}^{A}(k'), \tag{4}$$

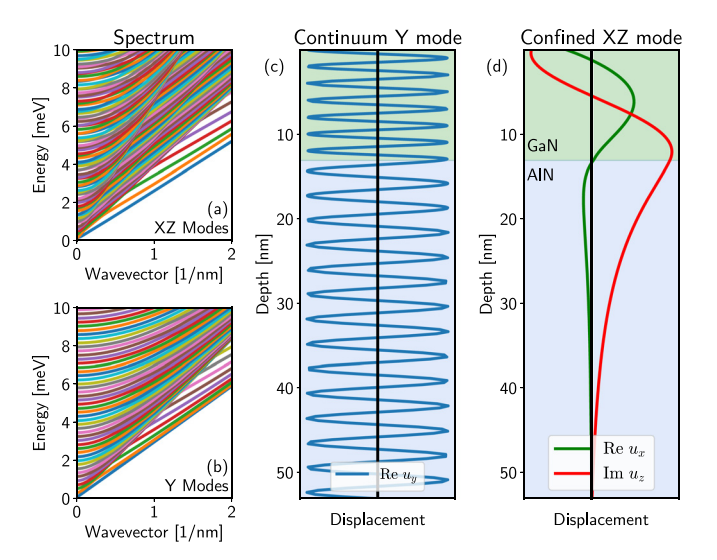


**FIG. 3.** Acoustic phonons. Spectrum of the (a) XZ polarized and (b) Y polarized modes. In each, there is a characteristic velocity dividing discrete modes and continuum modes:  $\sqrt{C_{44}/\rho}$  and  $\sqrt{(C_{11}-C_{12})/2\rho}$ , respectively. (c) An example of a continuum Y mode: oscillations are more concentrated in the GaN where the higher density leads to lower sound velocity. The lower sound velocity of GaN relative to AIN also allows for confinement, such as in (d), which depicts a confined XZ mode.

where  $\vec{\mathcal{E}}$  is the in-plane electric field,  $f^0$  is the equilibrium occupation function,  $f^A$  is a small change in occupation to be solved for, and the transition rate R is given by

$$R_{km}^{k'm'} = \frac{2\pi}{\hbar} \sum_{\alpha l} |\langle \psi_{k'm'} | H^l(q) | \psi_{km} \rangle|^2$$

$$\times \left( N + \frac{1}{2} (1 - \alpha) + \alpha f_{m'}^0(k') \right)$$

$$\times \delta(E_{k'm'} - E_{km} - \alpha \varepsilon_l(q)), \tag{5}$$

where  $\alpha=\pm 1$  represents the absorption/emission, respectively,  $\psi_{km}$  is the state with in-plane wavevector  $\vec{k}$ , of subband m,  $H^l(q)$  is the perturbation due to mode l with wavevector  $\vec{q}=\vec{k}'-\vec{k}$ , and  $E/\varepsilon$  are the electronic/phonon energies. Once this is discretized on a k-space mesh, the LBTE is solved as a linear matrix equation for the change in occupation  $\partial f^A/\partial \mathcal{E}$  under an applied field, from which the mobility is extracted. The results, Fig. 4, compare agreeably to experiment over a wide temperature range and verify Poncé's prediction  $^{17}$  that acoustic phonons dominate scattering at room temperature.

Now, we discuss what can be done to improve the mobility. In a recent first-principles study of the mobility of bulk p-type GaN, Poncé *et al.*<sup>17</sup> suggested the application of significant tensile in-plane strain (or compressive c-axis strain) to raise the split-off band (SO) above the

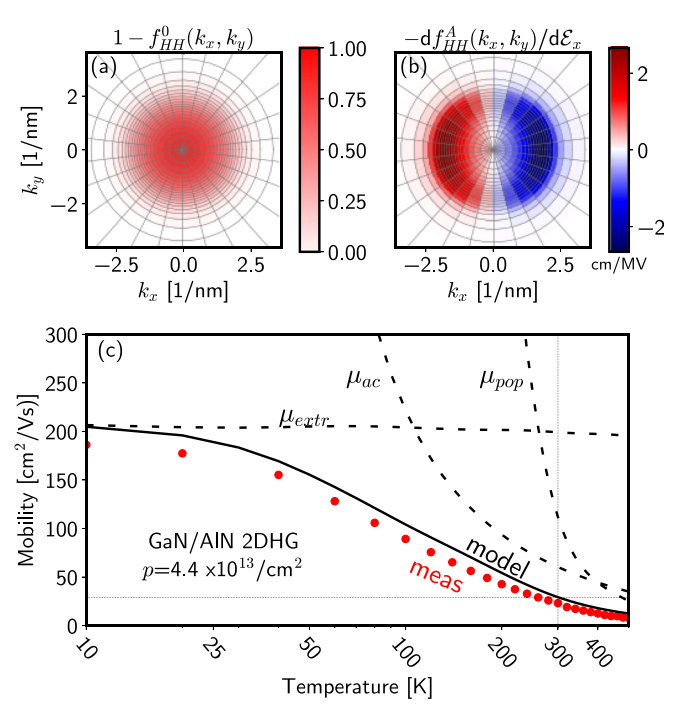


**FIG. 4.** (a) The hole occupation of the HH band at equilibrium and (b) the antisymmetric change in occupation per applied electric field in the +x direction, obtained by direct solution of the linearized Boltzmann Transport Equation. (The hole population is enhanced at negative  $k_x$ , which, given the negative group velocity for holes, implies a rightward current.) (c) Model mobility vs Hall measurements reported by Chaudhuri *et al.* Dashed curves are also shown for the various scattering mechanisms alone (polar optical, acoustic, and extrinsic). Note: the model is obtained by a full solution incorporating all mechanisms simultaneously, not by a Matthiessen approximation of the component limitations.

heavy-hole and light-hole bands. The lighter mass of the split-off band would allow for a drastically increased hole mobility. Such a proposal, while potentially revolutionary for bulk p-GaN, is difficult to apply to the particular heterostructure discussed here-in, since the GaN-pseudomorphic-to-AlN is already compressively strained by 2.4% asgrown and that large strain would have to be overcome first before applying further tensile strain. Moreover, applying tensile strain dramatically changes the interface between GaN and AlN, significantly reducing the valence band offset (VBO) and thus the confining potential. (The role of strain in the asymmetry of the GaN/AlN and AlN/GaN VBO is well-known.)<sup>35</sup>

This raises the question of whether reasonable strain can improve the mobility of holes in this heterostructure, without access to the deep SO band. Based on the theory of Suzuki and Uenoyama<sup>36</sup> in the context of lasers, two converse techniques may be suggested employing strain along only one in-plane axis. Dasgupta et al. 37 considered the application of compressive strain along the direction of current flow. Conversely, Gupta et al.38 tested the application of tensile strain perpendicular to current flow. Figures 5 and 6 consider what effects these two proposals have, not on bulk p-GaN as with previous authors but rather on the heterojunction band structure. To take full advantage of the changing band structure near the band edge, the charge density is lowered (by thinning the well layer to 8 nm) and kept constant at  $1 \times 10^{13}$ /cm<sup>2</sup> by variable applied bias even as the strain is changed. These adjustments to thickness and charge match closely the actual 2DHG environment in p-channel FETs.8 In parts (b) and (c) of these figures, uniaxial in-plane strain is seen to split the topmost two-bands. Depending on the sign and orientation of the strain, the topmost band may become light or heavy in the current flow direction (x).

In the case of tensile x-strain, Fig. 5(c), or compressive y-strain, Fig. 6(b), the topmost band is heavy along x, and so even though the available scattering DOS is reduced by the band-splitting, the net mobility remains low. However, in the case of compressive x-strain, Fig. 5(b), or tensile y strain, Fig. 6(c), the topmost band is light along x and interband scattering is diminished. As such, these strain

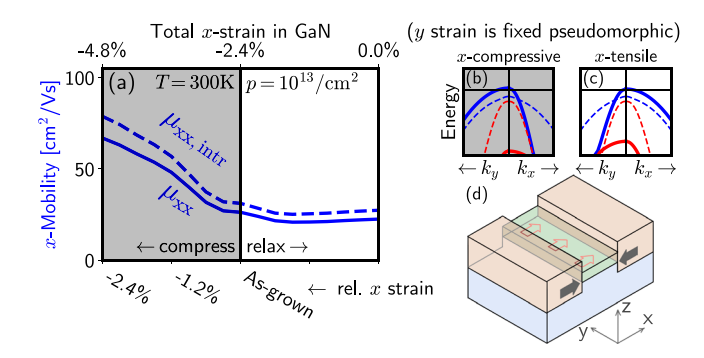


**FIG. 5.** (a) *x*-directed mobility due to all mechanisms (solid blue) and phonons only (dashed blue) vs strain along the current-flow direction (x). The y-direction is left pseudomorphic (-2.4% y-strain in GaN). Bottom axis: x-strain applied to structure. Top axis: corresponding total x-strain in GaN. For compressive x-strain, the x-directed mobility is enhanced. The dispersion along is shown under (b) compression and (c) tension as solid curves (dashed as-grown bands provided for comparison). The x-directed mobility enhancement corresponds to a reduced effective mass along  $k_x$  of the topmost band in (b). (d) Such compression could be applied, for example, by regrown stressors on the source and drain.

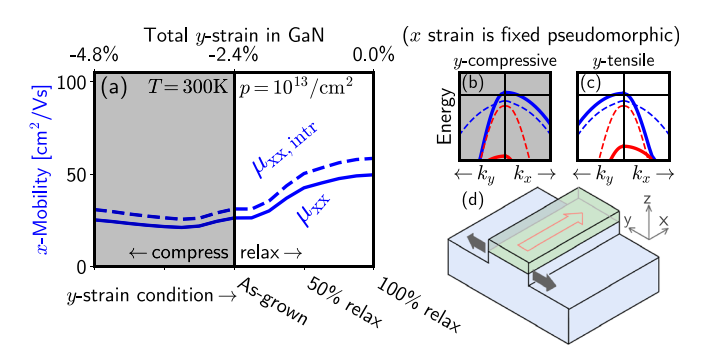


**FIG. 6.** Similar display as Fig. 5 but for strain applied "perpendicular" (y) to current flow (x). The x-direction is left pseudomorphic (-2.4% x-strain in GaN). (a) Tensile y-strain provides a mobility enhancement, corresponding to (c) a lighter effective mass along x. The bottom axis of (a) describes the tensile condition in terms of a unidirectional relaxation of the GaN strain perpendicular to current flow, as indicated by the fin release geometry of (d).

conditions result in an enhanced mobility. The mobility improvement due to *x*-compressive strain is more pronounced than that due to *y*-tensile strain because of the aforementioned effect which tensile strain has on the VBO. However, these two enhancement mechanisms are not mutually exclusive: a fin relaxation and a compressive regrowth would complement each other via the Poisson effect to reduce the total amount of stress which each mechanism would have to apply.

Of course, any enhancements will still be limited by whatever extrinsic mechanisms are at play, and so Figs. 5 and 6 include two mobility curves: (1) a (solid blue) prediction which assumes the extrinsic scattering element is similar to the present data and (2) a (dashed blue) intrinsic calculation using only phonon mechanisms, corresponding to space for further improvements in growth.

In conclusion, this work has combined solutions for both the optical and acoustic phonon spectra in a GaN/AlN heterostructure with a multiband description of the hole gas to model the hole mobility. The model qualitatively matches experimental observations and can be used to estimate what sort of intrinsic mobility enhancements are possible by strain engineering, suggesting that a unixial compression is the best approach for optimizing the GaN/AlN hole gas. A high-mobility 2DHG could join the celebrated GaN 2DEG to realize the future of energy-efficient complementary GaN-based circuits.

See the supplementary material for mathematical and numerical simulation details.

This work was supported by Intel Corp, by AFOSR Grant No. FA9550-17-1-0048, and by NSF Grant Nos. 1710298/1534303. The authors appreciate discussions with Samuel Poncé, Feliciano Giustino, Tomás Palacios, Nadim Chowdhury, Paul Fischer, and Sansaptak Dasgupta.

#### **REFERENCES**

<sup>1</sup>S. Nakamura, T. Mukai, M. Senoh, and N. Iwasa, "Thermal annealing effects on P-type Mg-doped GaN films," Jpn. J. App. Phys. Part 2 **31**, L139 (1992).

<sup>2</sup>A. Q. Huang, "Wide bandgap (WBG) power devices and their impacts on power delivery systems," in Technical Digest: International Electron Devices Meeting, IEDM (2017), p. 20.1.1.1.4.

- <sup>3</sup>K. Yuk, G. R. Branner, and C. Cui, "Future directions for GaN in 5G and satellite communications," in 2017 Midwest Symposium on Circuits and Systems (2017), p. 803.
- <sup>4</sup>J. O. Song, J. S. Ha, and T. Y. Seong, "Ohmic-contact technology for GaN-based light-emitting diodes: Role of p-type contact," IEEE Trans. Electron Devices 57, 42 (2010).
- <sup>5</sup>P. Kozodoy, H. Xing, S. P. DenBaars, U. K. Mishra, A. Saxler, R. Perrin, S. Elhamri, and W. C. Mitchel, "Heavy doping effects in Mg-doped GaN," J. Appl. Phys. **87**, 1832 (2000).
- <sup>6</sup>R. Chu, Y. Cao, M. Chen, R. Li, and D. Zehnder, "An experimental demonstration of GaN CMOS technology," IEEE Electron Device Lett. 37, 269 (2016).
- <sup>7</sup>R. Chaudhuri, S. J. Bader, Z. Chen, D. A. Muller, H. G. Xing, and D. Jena, "A polarization-induced 2D hole gas in undoped gallium nitride quantum wells," e-print arXiv:1807.08836.
- 8S. J. Bader, R. Chaudhuri, K. Nomoto, A. Hickman, Z. Chen, H. W. Then, D. A. Muller, H. G. Xing, and D. Jena, "Gate-recessed E-mode p-channel HFET with high on-current based on GaN/AlN 2D hole gas," IEEE Electron Device Lett. 39, 1848 (2018).
- <sup>9</sup>M. Shatalov, G. Simin, J. Zhang, V. Adivarahan, A. Koudymov, R. Pachipulusu, and M. A. Khan, "GaN/AlGaN p-channel inverted heterostructure JFET," IEEE Electron Device Lett. 23, 452 (2002).
- <sup>10</sup>T. Zimmermann, M. Neuburger, M. Kunze, I. Daumiller, A. Denisenko, A. Dadgar, A. Krost, and E. Kohn, "P-channel InGaN-HFET structure based on polarization doping," IEEE Electron Device Lett. 25, 450 (2004).
- <sup>11</sup>G. Li, R. Wang, B. Song, J. Verma, Y. Cao, S. Ganguly, A. Verma, J. Guo, H. G. Xing, and D. Jena, "Polarization-induced GaN-on-insulator E/D mode p-channel heterostructure FETs," IEEE Electron Device Lett. 34, 852 (2013).
- <sup>12</sup>H. Hahn, B. Reuters, A. Pooth, B. Hollander, M. Heuken, H. Kalisch, and A. Vescan, "P-channel enhancement and depletion mode GaN-based HFETs with quaternary backbarriers," IEEE Trans. Electron Devices 60, 3005 (2013).
- <sup>13</sup>K. Zhang, M. Sumiya, M. Liao, Y. Koide, and L. Sang, "P-channel InGaN/GaN heterostructure metal-oxide-semiconductor field effect transistor based on polarization-induced two-dimensional hole gas," Sci. Rep. 6, 23683 (2016).
- 14<sup>t</sup>K. Nomoto, S. J. Bader, K. Lee, S. Bharadwaj, Z. Hu, H. G. Xing, and D. Jena, "Wide-bandgap gallium nitride p-channel MISFETs with enhanced performance at high temperature," in Device Research Conference: Conference Digest, DRC (2017).
- <sup>15</sup>A. Nakajima, S. Kubota, K. Tsutsui, K. Kakushima, H. Wakabayashi, H. Iwai, S.-I. Nishizawa, and H. Ohashi, "GaN-based complementary metal-oxide-semiconductor inverter with normally off Pch and Nch MOSFETs fabricated using polarisation-induced holes and electron channels," IET Power Electron. 11, 689 (2018).
- 16 A. Krishna, A. Raj, N. Hatui, B. Romanczyk, and O. Koksaldi, "Gallium nitride (GaN) superlattice (SL) based p-channel field effect transistor," preprint arXiv:1902.02022 (2019).
- <sup>17</sup>S. Ponce, D. Jena, and F. Giustino, "First demonstration of Aluminum gallium nitride (AlGaN) - Gallium nitride (GaN) superlattice (SL) based p-channel field effect transistor" (unpublished).
- <sup>18</sup>B. A. Foreman, "Effective-mass Hamiltonian and boundary conditions for the valence bands of semiconductor microstructures," Phys. Rev. B 48, 4964 (1993).

- <sup>19</sup>M. G. Burt, "Direct derivation of effective-mass equations for microstructures with atomically abrupt boundaries," Phys. Rev. B 50, 7518 (1994).
- <sup>20</sup>F. Mireles and S. Ulloa, "Ordered Hamiltonian and matching conditions for heterojunctions with wurtzite symmetry: (formula presented) quantum wells," Phys. Rev. B: Condens. Matter Mater. Phys. 60, 13659 (1999).
- <sup>21</sup>S. L. Chuang and C. S. Chang, "KP method for strained wurtzite semi-conductors," Phys. Rev. B 54, 2491–2504 (1996).
- 22S. Birner, "Modeling of semiconductor nanostructures and semiconductor-electrolyte interfaces," Ph.D. thesis (Technical University of Munich, 2011).
- <sup>23</sup>S. J. Bader, see http://sambader.net/pynitride for "PyNitride."
- <sup>24</sup>I.-H. Tan, G. L. Snider, L. D. Chang, and E. L. Hu, "A self-consistent solution of Schrodinger-Poisson equations using a nonuniform mesh," J. Appl. Phys. 68, 4071 (1990).
- <sup>25</sup>M. A. Stroscio and M. Dutta, *Phonons in Nanostructures* (Cambridge University Press, Cambridge, 2004).
- <sup>26</sup>J. Shi, "Interface optical-phonon modes and electroninterface-phonon interactions in wurtzite GaN/AlN quantum wells," Phys. Rev. B 68, 165335 (2003).
- 27S. K. Medeiros, E. L. Albuquerque, G. A. Farias, M. S. Vasconcelos, and D. H. A. L. Anselmo, "Confinement of polar optical phonons in AlN/GaN superlattices," Solid State Commun. 135, 144 (2005).
- <sup>28</sup>S. Liao, M. Dutta, and M. A. Stroscio, "Interface optical phonon modes in wurtzite quantum heterostructures," in 2010 International Workshop on Computational Electronics (2010), Vol. 215, p. 054312.
- <sup>29</sup>S. Komirenko, K. Kim, M. Stroscio, and M. Dutta, "Dispersion of polar optical phonons in wurtzite quantum wells," Phys. Rev. B 59, 5013 (1999).
- 30 J. Zhu, S. L. Ban, and S. H. Ha, "Phonon-assisted intersubband transitions in wurtzite GaN/In<sub>x</sub>Ga<sub>1-x</sub>N quantum wells," Chin. Phys. B 21, 097301 (2012).
- <sup>31</sup>E. P. Pokatilov, D. L. Nika, and A. A. Balandin, "Phonon spectrum and group velocities in AlN/GaN/AlN and related heterostructures," Superlattices Microstruct. 33, 155 (2003).
- <sup>32</sup>E. P. Pokatilov, D. L. Nika, and A. A. Balandin, "Confined electron-confined phonon scattering rates in wurtzite AlN/GaN/AlN heterostructures," J. Appl. Phys. 95, 5626 (2004).
- 33A. A. Balandin, D. L. Nika, and E. P. Pokatilov, "Phonon spectrum and group velocities in wurtzite hetero-structures," Phys. Status Solidi C 1, 2658 (2004).
- 34A. A. Balandin, E. P. Pokatilov, and D. L. Nika, "Phonon engineering in heteroand nanostructures." J. Nanoelectron. Optoelectron. 2, 140 (2007).
- 35I. Vurgaftman and J. R. Meyer, "Band parameters for nitrogen-containing semiconductors," J. Appl. Phys. 94, 3675 (2003).
- <sup>36</sup>M. Suzuki and T. Uenoyama, "Reduction of threshold current density of wurtzite GaN/AlGaN quantum well lasers by uniaxial strain in (0001) plane," Jpn. J. Appl. Phys. Part 2 35, L953 (1996).
- 37 S. Dasgupta, M. Radosavljevic, and H. W. Then, "Stressors for compressively strained GaN p-channel," U. S. patent WO 2017/099752 Al 15 (15 June 2017)
- <sup>38</sup>C. Gupta, Y. Tsukada, B. Romanczyk, S. S. Pasayat, D.-A. James, S. Keller, and U. K. Mishra, "First experimental demonstration of enhancement in hole conductivity in c-plane (0001) III-nitrides with uniaxial strain," in International Workshop on Nitrides, Kanazawa, Japan (2018).

# Supplement to "Wurtzite Phonons and the Mobility of a GaN/AlN 2D Hole Gas"

# S1) Multiband kp model

The Multiband k.p matrix differential equation<sup>1</sup> can be split into four terms by the order of derivatives

$$\left[C^{0}(z) - iC^{L}(z)\partial_{z} - i\partial_{z}C^{R}(z) - \partial_{z}C^{2}(z)\partial_{z}\right]f(z) = \lambda f(z) \tag{S1}$$

where, for a wurtzite valence band f(z) is a six-component spinor. In the basis  $|X\uparrow\rangle, |Y\uparrow\rangle, |Z\uparrow\rangle, |X\downarrow\rangle, |Y\downarrow\rangle, |Z\downarrow\rangle$ , these position-dependent matrices can be written

$$C^0 = C^{0L} + C^{0D} + C^{0S} (S2)$$

$$C^{0L} = I_{2} \otimes \begin{pmatrix} k_{x}L_{1}^{u}k_{x} + k_{y}M_{1}^{u}k_{y} & k_{x}N_{1}^{+}k_{y} + k_{y}N_{1}^{-}k_{x} & \cdot \\ k_{y}N_{1}^{+}k_{x} + k_{x}N_{1}^{-}k_{y} & k_{x}M_{1}^{u}k_{x} + k_{y}L_{1}^{u}k_{y} & \cdot \\ & \cdot & k_{x}M_{3}^{u}k_{x} + k_{y}M_{3}^{u}k_{y} \end{pmatrix}$$
(S3)

$$C^{0D} = \begin{pmatrix} \Delta_1 & -i\Delta_2 & \cdot & \cdot & \cdot & \Delta_3 \\ i\Delta_2 & \Delta_1 & \cdot & \cdot & \cdot & -i\Delta_3 \\ \cdot & \cdot & \cdot & -\Delta_3 & i\Delta_3 & \cdot \\ \cdot & \cdot & -\Delta_3 & \Delta_1 & i\Delta_2 & \cdot \\ \cdot & \cdot & -i\Delta_3 & -i\Delta_2 & \Delta_1 & \cdot \\ \Delta_3 & i\Delta_3 & \cdot & \cdot & \cdot & \cdot \end{pmatrix}$$
 (S4)

$$C^{0S} = \begin{pmatrix} l_1 e_{xx} + m_1 e_{yy} + m_2 e_{zz} & n_1 e_{xy} & n_2 e_{xz} \\ n_1 e_{xy} & m_1 e_{xx} + l_1 e_{yy} + m_2 e_{zz} & n_2 e_{yz} \\ n_2 e_{xz} & n_2 e_{yz} & m_3 e_{xx} + m_3 e_{yy} + l_2 e_{zz} \end{pmatrix}$$
(S5)

$$C^{L} = I_{2} \otimes \begin{pmatrix} \cdot & \cdot & k_{x} N_{2}^{+} \\ \cdot & \cdot & k_{y} N_{2}^{+} \\ k_{x} N_{2}^{-} & k_{y} N_{2}^{-} & \cdot \end{pmatrix}$$
 (S6)

$$C^{R} = I_{2} \otimes \begin{pmatrix} \cdot & \cdot & N_{2}^{-}k_{x} \\ \cdot & \cdot & N_{2}^{-}k_{y} \\ N_{2}^{+}k_{x} & N_{2}^{+}k_{y} & \cdot \end{pmatrix}$$
 (S7)

$$C^{2} = I_{2} \otimes \begin{pmatrix} M_{2}^{u} & \cdot & \cdot \\ \cdot & M_{2}^{u} & \cdot \\ \cdot & \cdot & L_{2}^{u} \end{pmatrix}$$
 (S8)

where  $I_2$  is the 2x2 identity matrix,

$$L_1^u = A_2 + A_4 + A_5, \quad L_2^u = A_1$$
 
$$M_1^u = A_2 + A_4 - A_5, \quad M_2^u = A_1 + A_3, \quad M_3^u = A_2$$
 
$$N_1^+ = 3A_5 - A_2 - A_4 + U; \quad N_1^- = -A_5 + A_2 + A_4 - U$$
 
$$N_2^+ = \sqrt{2}A_6 - A_1 - A_3 + U, \quad N_2^- = A_1 + A_3 - U$$

with  $U = \frac{\hbar^2}{2m_e}$  and

$$l_1 = D_2 + D_4 + D_5, \quad l_2 = D_1$$
  $m_1 = D_2 + D_4 - D_5, \quad m_2 = D_1 + D_3, \quad m_3 = D_2$   $n_1 = 2D_5, \quad n_2 = \sqrt{2}D_6$ 

where  $A_i$  are the Rashba-Sheka-Pikus parameters and  $D_i$  are the deformation potentials. Notes:

- The  $A_7$  parameter is neglected as is common in heterostructural multiband kp analysis<sup>1</sup>. The effects of this negligence are known<sup>8</sup>
- Since none of the important scattering mechanisms interact with spin and the spin-splitting is a small energy scale in the band structure, one can "cheat" that degree of freedom to speed up calculations. For faster evaluation of mobility, the off-diagonal 3x3 blocks of  $C_{0D}$  are zeroed and a sub-meV up-down term is added along the diagonal to ensure the spins have a finite non-degeneracy. Then the mobility calculation can account for only one of the spins and assume the same for the other.
- The above calculation is a 6x6 kp method in which the valence bands are accounted for directly and the conduction band appears only as a perturbation. Since GaN is a wide-bandgap material, this convenient simplification is reasonably accurate as compared to a slower 8x8 kp implementation.

# S2) Acoustic phonon dispersion

As given in the main text, the elastic continuum model joins the continuum Newton's law with the material stress-strain relation<sup>7</sup>:

$$\rho \frac{\partial^2 u_i}{\partial t^2} = \frac{\partial T_{ij}}{\partial r_i}, \quad T_{ij} = c_{ijkl} \epsilon_{kl}$$
 (S9)

where  $u_i$  is the local displacement,  $\rho$  is the density,  $T_{ij}$  is the stress tensor,  $c_{ijkl}$ is the stiffness tensor, and  $\epsilon_{ijkl}$  is the strain tensor  $\epsilon_{ij} = \frac{1}{2} \left( \partial_{r_j} u_i + \partial_{r_i} u_j \right)$ . The latter equation can be re-expressed in Voigt notation

$$T_{\alpha} = c_{\alpha\beta}\epsilon_{\beta} \tag{S10}$$

where  $\alpha, \beta$  run 1-6 and the Voigt tuples are related to the actual tensors by

$$T_1 = T_{xx}, \quad \epsilon_1 = \epsilon_{xx}$$
 (S11)

$$T_2 = T_{yy}, \quad \epsilon_2 = \epsilon_{yy}$$
 (S12)

$$T_3 = T_{zz}, \quad \epsilon_3 = \epsilon_{zz}$$
 (S13)

$$T_4 = T_{yz}, \quad \epsilon_4 = 2\epsilon_{yz}$$
 (S14)

$$T_5 = T_{xz}, \quad \epsilon_5 = 2\epsilon_{xz}$$
 (S15)

$$T_6 = T_{xy}, \quad \epsilon_6 = 2\epsilon_{xy}$$
 (S16)

For a wurtzite crystal, the  $c_{\alpha\beta}$  can be written

$$c = \begin{pmatrix} C_{11} & C_{12} & C_{13} & 0 & 0 & 0 \\ C_{12} & C_{22} & C_{13} & 0 & 0 & 0 \\ C_{13} & C_{13} & C_{33} & 0 & 0 & 0 \\ 0 & 0 & 0 & C_{44} & 0 & 0 \\ 0 & 0 & 0 & 0 & C_{44} & 0 \\ 0 & 0 & 0 & 0 & 0 & \frac{1}{2} \left( C_{11} - C_{12} \right) \end{pmatrix}$$
 (S17)

For a wurtzite structure uniform in the basal plane but possibly inhomogenous along z, we note that the elastic continuum model is rotationally symmetric in plane, so we can choose the in-plane wavevector along x and assume phonons have a form

$$u = \begin{pmatrix} u_x(z) \\ u_y(z) \\ u_z(z) \end{pmatrix} e^{i(qx - \omega t)}$$
 (S18)

We will hide the explicit z dependence for now. The the strain can be evaluated

$$\epsilon_1 = iqu_x, \qquad \qquad \epsilon_4 = \partial_z u_y \qquad (S19)$$
 $\epsilon_2 = 0, \qquad \qquad \epsilon_5 = iqu_z + \partial_z u_x \qquad (S20)$ 
 $\epsilon_3 = \partial_z u_z, \qquad \qquad \epsilon_6 = iqu_y \qquad (S21)$ 

$$\epsilon_2 = 0,$$
  $\epsilon_5 = iqu_z + \partial_z u_x$  (S20)

$$\epsilon_3 = \partial_z u_z, \qquad \qquad \epsilon_6 = iqu_y$$
 (S21)

Then the two constitutive laws can be combined as

$$-\rho\omega^{2}\begin{pmatrix}u_{x}\\u_{y}\\u_{z}\end{pmatrix} = \begin{pmatrix}-C_{11}q^{2}u_{x} + iqC_{13}\partial_{z}u_{z} + \partial_{z}C_{44}iqu_{z} + \partial_{z}C_{44}\partial_{z}u_{x}\\ -\frac{1}{2}\left(C_{11} - C_{12}\right)q^{2}u_{y} + \partial_{z}C_{44}\partial_{z}u_{y}\\ -C_{44}q^{2}u_{z} + C_{44}iq\partial_{z}u_{x} + iq\partial_{z}C_{13}u_{x} + \partial_{z}C_{33}\partial_{z}u_{z}\end{pmatrix}$$
(S22)

This matrix can be split by order

$$\rho \omega^2 u = Cu, \quad C = q^2 C^0 - iq C^L \partial_z - iq \partial_z C^R - \partial_z C^2 \partial_z$$
 (S23)

where

$$C^{0} = \begin{pmatrix} C_{11} & & \\ & \frac{1}{2} \left( C_{11} - C_{12} \right) & \\ & C_{44} \end{pmatrix}, \quad C^{2} = \begin{pmatrix} C_{44} & & \\ & C_{44} & \\ & & C_{33} \end{pmatrix}$$
 (S24)

$$C^{L} = \begin{pmatrix} & C_{13} \\ & 0 \\ & \\ C_{44} & \end{pmatrix}, \quad C^{R} = \begin{pmatrix} & C_{44} \\ & 0 \\ & \\ C_{13} & \end{pmatrix}$$
 (S25)

This generalized eigenvalue problem can be solved by the Finite Element Method once boundary conditions are prescribed. Specifically, the upper boundary will be treated as free to vibrate (i.e. Neumann), so  $T_{iz} = 0$ . The bottom boundary is unimportant in the limit of a thick buffer, but, to preclude the appearance of an irrelevant bottom-boundary mode decaying upwards into AlN, one may set the bottom boundary by Dirichelet  $u_i = 0$  condition.

We note here that in the above matrices, there is no coupling between the Y (second) component and the XZ (first and third) components, so the problem could be further broken apart into a pair of problems if desired.

#### S2.1) Piezoelectric potential

Once the acoustic phonon modes are solved for, each mode can be considered a source of piezoelectric charge, which induces a further scattering potential. This approximation of treating the acoustic and electric problem separately is common practice<sup>6</sup> given the low-frequency of zone-center acoustic phonons. A phonon in a piezoelectric material induces a charge

$$\rho = -\nabla \cdot \vec{P} = -\nabla \cdot \begin{bmatrix} 0 & 0 & 0 & e_{15} & 0 \\ 0 & 0 & 0 & e_{15} & 0 & 0 \\ e_{31} & e_{31} & e_{33} & 0 & 0 & 0 \end{bmatrix} \begin{pmatrix} \epsilon_{xx} \\ \epsilon_{yy} \\ \epsilon_{zz} \\ 2\epsilon_{yz} \\ 2\epsilon_{xz} \\ 2\epsilon_{xy} \end{bmatrix}$$
(S26)

where  $e_{\alpha\beta}$  are the piezoelastic moduli

$$= -\nabla \cdot \begin{pmatrix} e_{15}\epsilon_{xz} \\ e_{15}\epsilon_{yz} \\ e_{31}\epsilon_{xx} + e_{31}\epsilon_{yy} + e_{33}\epsilon_{zz} \end{pmatrix}$$
 (S27)

$$= -e_{15}(iq_x\epsilon_{xz} + iq_y\epsilon_{yz}) - \partial_z[e_{31}(\epsilon_{xx} + \epsilon_{yy}) + e_{33}\epsilon_{zz}]$$
 (S28)

$$= -e_{15}(iq_x\partial_z u_x - q_x^2 u_z + iq_y\partial_z u_y - q_y^2 u_z)$$
(S29)

$$-\partial_z[ie_{31}(q_xu_x + q_yu_y) + e_{33}\partial_zu_z]$$
 (S30)

$$= -e_{15}(iq\partial_z u_L - q^2 u_z) - \partial_z[iqe_{31}u_L + e_{33}\partial_z u_z]$$
 (S31)

$$= q^2 e_{15} u_z - iq e_{15} \partial_z u_L - iq \partial_z e_{31} u_L - \partial_z e_{33} \partial_z u_z$$
 (S32)

where  $u_L$  is the in-plane longitudinal component of the displacement. Plugging this into the Poisson equation, we find a potential

$$-\nabla \left[\varepsilon \nabla \phi\right] = \rho \tag{S33}$$

$$q^2 \varepsilon_{\perp} \phi - \partial_z \varepsilon_{\parallel} \partial_z \phi = \rho \tag{S34}$$

So

$$q^{2}\varepsilon_{\perp}\phi - \partial_{z}\varepsilon_{\parallel}\partial_{z}\phi = q^{2}e_{15}u_{z} - iqe_{15}\partial_{z}u_{L} - iq\partial_{z}e_{31}u_{L} - \partial_{z}e_{33}\partial_{z}u_{z}$$
 (S35)

which can be written

$$C^{0}\phi - \partial_{z}C^{2}\partial_{z}\phi = C^{0'}u_{z} - iC^{L'}\partial_{z}u_{x} - i\partial_{z}C^{R'}u_{x} - \partial_{z}C^{2'}\partial_{z}u_{z}$$
 (S36)

where

$$C_0 = q^2 \varepsilon_{\perp}, \quad C_2 = \varepsilon_{\parallel}$$
 (S37)

$$C^{0'} = q^2 e_{15}, C^{L'} = q e_{15}, C^{R'} = q e_{31}, C^{2'} = e_{33}$$
 (S38)

and solved by the Finite Element Method.

### S3) Polar optical phonon dispersion

As discussed in the main text, the interaction of the uniaxial polar atomic lattice with electromagnetic waves can be incorporated as a pair of frequency-dependent dielectric constants  $\varepsilon_{\parallel}$  and  $\varepsilon_{\perp}$ , upon which solving the Poisson equation gives all the modes which produce an electric potential [that is, all the modes which are important for POP scattering]. For in-plane wavevector q,

$$\partial_z \epsilon_{\parallel} \partial_z \phi = q^2 \epsilon_{\perp} \phi \tag{S39}$$

The normalization condition given in the main text, applied to both classes of phonon, is expressed in terms of u, but, by solving for u as a function of  $\phi$ , this condition can be re-expressed directly in terms of  $\phi$ :

$$\frac{\hbar}{2\omega} = \int dz \varepsilon_{\infty} (\omega_{LO}^2 - \omega_{TO}^2) \left( \left( \frac{\partial_z \phi}{\omega_{TO\parallel}^2 - \omega^2} \right)^2 + \left( \frac{q\phi}{\omega_{TO\perp}^2 - \omega^2} \right)^2 \right)$$
 (S40)

Given the frequency-dependence of the parameters in the equation, a numerical solution of the eigenvalue problem is actually somewhat involved. Fortunately, the discretely layered binary heterostructure structure lends itself to analytic solutions. We will solve a single heterojunction structure 1/2 where materials 1 and 2 are GaN or AlN in either order, and the bottom material is semi-infinite. The top surface at z=0 is assumed Dirichelet. The thickness of the top layer is  $t_1$  and a normalization thickness of  $t_2$  is set for the bottom layer which will discretize the bottom-region-confined states.

In a given region, solutions are oscillating if  $\varepsilon_{\perp}\varepsilon_{\parallel} < 0$  and exponential if  $\varepsilon_{\perp}\varepsilon_{\parallel} > 0$ . At an interface, the derivative switches signs iff  $\varepsilon_{1\parallel}\varepsilon_{2\parallel} < 0$ . We will use the following convenient definitions, similar to the notation of Komirenko<sup>5</sup> but for a factor of two in  $\alpha$ 

$$\xi_i = \sqrt{\left|\varepsilon_{i\perp}\varepsilon_{i\parallel}\right|}, \quad \alpha_i = \sqrt{\left|\varepsilon_{i\perp}/\varepsilon_{i\parallel}\right|}$$
 (S41)

Then the vertical wavevector of a mode in a given region is  $k_i = q\alpha_i$ .

If the solution is written in Region 1 with some normalization constant A and Region 2 with some normalization constant B, then the first matching condition  $\phi(t_1^-) = \phi_2(t_1^+)$  gives us some expression for B/A, and the normalization condition will be written for A:

$$A^{2} = \frac{\hbar}{2\omega} / \left[ \beta_{\parallel 1}^{2} \gamma_{\parallel 1}^{2} + \beta_{\perp 1}^{2} \gamma_{\perp 1}^{2} + \left( \frac{B}{A} \right)^{2} \left( \beta_{\parallel 2}^{2} \gamma_{\parallel 2}^{2} + \beta_{\perp 2}^{2} \gamma_{\perp 2}^{2} \right) \right]$$
 (S42)

with

$$\beta_{\parallel i}^2 = \varepsilon_i^{\infty} \left( \omega_{LOi}^2 - \omega_{TOi}^2 \right) \left( \frac{k_i}{\omega_{TO\parallel i}^2 - \omega^2} \right)^2 \tag{S43}$$

$$\beta_{\perp i}^2 = \varepsilon_i^{\infty} \left( \omega_{LOi}^2 - \omega_{TOi}^2 \right) \left( \frac{q}{\omega_{TO\perp i}^2 - \omega^2} \right)^2$$
 (S44)

and

$$\gamma_{\parallel i}^2 = \int_i dz \left(\frac{\partial_z \phi}{A k_i}\right)^2, \quad \gamma_{\perp i}^2 = \int_i dz \left(\frac{\phi}{B}\right)^2$$
 (S45)

From there on out, the solution is a simple mechanical procedure, depending on the signs of the dielectric constants.

#### S3.1) Confined to Region 1

If the solution is oscillating in Region 1 and decaying in Region 2, we can write

$$\phi_1 = A\sin(k_1 z), \quad \phi_2 = Be^{-k_2 z}$$
 (S46)

Matching interface conditions gives

$$q = \frac{1}{\alpha_1 t_1} \left[ \tan^{-1} \left( \xi_1 / \xi_2 \right) + \pi n \right]$$
 (S47)

with  $B/A = \sin(k_1 t_1) e^{k_2 t_1}$  and

$$\gamma_{\parallel 1} = \frac{1}{2}(t_1 + \frac{1}{2k_1}\sin(2k_1t_1)), \quad \gamma_{\perp 1} = \frac{1}{2}(t_1 - \frac{1}{2k_1}\sin(2k_1t_1))$$
(S48)

$$\gamma_{\parallel 2} = \frac{1}{2k_2} e^{-2k_2 t_1}, \quad \gamma_{\perp 2} = \frac{1}{2k_2} e^{-2k_2 t_1}$$
(S49)

#### S3.2) Confined to Interface

If the solution is decaying in both regions, we can write

$$\phi_1 = A \sinh(k_1 z), \quad \phi_2 = B e^{-k_2 z}$$
 (S50)

Matching interface conditions gives

$$q = \frac{1}{2\alpha t_1} \log \left[ \frac{\xi_2 + \xi_1}{\xi_2 - \xi_1} \right] \tag{S51}$$

with  $B/A = \sinh(k_1t_1)e^{k_2t_1}$  and

$$\gamma_{\parallel 1} = \frac{1}{2} \left( \frac{1}{2k_1} \sinh(2k_1 t_1) + t_1 \right), \quad \gamma_{\perp 1} = \frac{1}{2} \left( \frac{1}{2k_1} \sinh(2k_1 t_1) - t_1 \right) \quad (S52)$$

$$\gamma_{\parallel 2} = \frac{1}{2k_2} e^{-2k_2 t_1}, \quad \gamma_{\perp 2} = \frac{1}{2k_2} e^{-2k_2 t_1}$$
(S53)

#### S3.3) Confined to Region 2

If the solution is decaying in Region 1 and oscillating in Region 2, we can write

$$\phi_1 = A \sinh(k_1 z), \quad \phi_2 = B \sin(k_2 z + \theta) \tag{S54}$$

Matching interface conditions gives

$$\theta = \tan^{-1}\left(\frac{\xi_2}{\xi_1}\tanh(k_1t_1)\right) - k_2t_1 \tag{S55}$$

with  $B/A = \sinh(k_1t_1)/\sin(k_2t_1+\theta)$ . The  $t_2$  thickness normalization gives  $k_2 = \pi(n+1)/t_2$ , so

$$q = \frac{\pi(n+1)}{\alpha_2 t_2} \tag{S56}$$

Normalization is accounted for via

$$\gamma_{\parallel 1} = \frac{1}{2} \left( \frac{1}{2k_1} \sinh(2k_1 t_1) + t_1 \right), \quad \gamma_{\perp 1} = \frac{1}{2} \left( \frac{1}{2k_1} \sinh(2k_1 t_1) - t_1 \right) \quad (S57)$$

$$\gamma_{\parallel 2} = \frac{t_2}{2}, \quad \gamma_{\perp 2} = \frac{t_2}{2}$$
(S58)

# S4) Numerical details

Most material parameters are drawn from Vurgaftman and Meyer's compilation<sup>11</sup>, but anisotropic dielectric constants are from the measurements of Kane<sup>3</sup> and Kazan<sup>4</sup>, optical phonon parameters are from the compilation in Komirenko<sup>5</sup> and the polarization-related quantities are computed from the calculations of Dreyer<sup>2</sup>. To ensure that the results do not depend on the specific choice of  $k \cdot p$ 

parameters, we performed the entire calculation with not only the  $k \cdot p$  parameters from Vurgaftman and Meyer but also ran a comparison with more recent parameters fitted by Rinke<sup>9</sup> from atomistic GW calculations (but keeping the  $\Delta_{SO}$  since Rinke neglects this). Results and trends were quite similar despite the differences in individual parameters.

The first step in each mobility point is calculation of the band diagram by a standard Newton iteration of a charge model (including analytical derivatives) and the Poisson equation (as laid out in Tan's work<sup>10</sup>). The Poisson equation includes a Dirichelet boundary at the surface (SBH of 1.4 eV) and a Neumann boundary at the artificial bottom termination (500nm of AlN). The charge density consists of polarization contributions (from the interface discontinuities), quantum carrier densities (from occupation of the MBKP-solved states in a region extending from the surface to several nanometers below the interface), classical carrier densities (from occupation of the band-edge DOS in a region extending from several nanometers below the interface down the rest of the domain), and a small background  $(1 \times 10^{17}/\text{cm}^3)$  of deep donor-like defects throughout. To achieve convergence over a wide range of conditions and temperatures despite extreme charges, the algorithm begins by artificially scaling up all dielectric constants by orders of magnitude to decouple the charge and fields, and then ramps the dielectric constants to their true values. For the simulations with varied strain, the Fermi level at the surface is adjusted (mimicking application of a gate) to keep the hole sheet density at a particular set value.

Separately, the phonon energies are evaluated by the means described in the above sections, with the caveat that the artificial bottom termination for the phonon solution domain is 40nm into the AlN (rather than 500nm as used for electrical simulation). This abridgment drastically reduces the time and storage requirements of the mobility solution, mainly by reducing the number of pseudo-continuum modes which must be considered, but is deep enough that the artificial confinement effects on the phonon spectra are at an energy scale well below thermal energy over the entire temperature range where phonons contribute significantly to scattering. Specifically, the phonon states used are the first 400 acoustic modes (including discrete and pseudo-continuum states indiscriminately), the first 20 AlN-confined optical modes of each polarization, the first 30 GaN-confined modes of each polarization, and both polarizations of the interface optical mode.

With both phonon and electron states solved, we then solve the Linearized Boltzmann Transport Equation. We first discretize k-space. In regions of k-space where the occupation changes rapidly with k (that is, essentially, regions within a  $k_bT$  scale of the Fermi energy and with significant group velocity), it is vital to define a dense grid. However, since this equation is to be solved over a wide range of temperatures and under many variations of the bandstructure, the precise locations of these important regions are not known in advance. Thus, an adaptive mesh is formed by the following procedure.

The mesh will be uniform in the  $\theta$  direction, but variably spaced along k. The derivative D of circularly averaged occupation with respect to k is calculated  $(D = \frac{1}{2\pi} \partial_k \int d\theta f(k, \theta))$ , and an upper bound  $k_{\text{max}}$  for the k-mesh is determined

by a point beyond which D has fallen off to a negligible value compared to its peak. The simplest strategy would be then to space mesh points evenly with respect to k from zero to this upper bound. A more aggressive strategy is to space mesh points evenly with respect to circularly averaged occupation, thus regions with a rapidly changing occupation have the higher density of points. For this work, a compromise is struck in which the k-points are placed evenly along a weighted average (.7+.3) of  $\frac{1}{2\pi}\int d\theta f(k,\theta)$  and  $k/k_{\rm max}$ , ensuring a spread of k-points which cluster around the vital regions. Employing this adaptive scheme, a relatively small grid of 25 k-values x 18  $\theta$  values (or, for simulations in which hexagonal symmetry broken, 25x24) was found sufficient. This is the mesh on which transition matrix elements will be calculated.

This mesh is further refined by even subdivision (here by a factor of 4) for the computation of the energy-conserving  $\delta$  function factor, a more rapidly varying factor of position. For each subcell, all the other subcells into which the centerpoint of that subcell may legally scatter are found, and the delta-function determinant is computed using k-derivatives evaluated at the subcell centers. These contributions over subcells are then summed to produce a sparse matrix of the conservation factors between each cell of the original mesh described in the previous paragraph. Then, on the original mesh, the necessary transition matrix elements can be calculated only where needed by the relevant interaction Hamiltonian and the two factors are multiplied.

Explicitly, those transition matrix elements, the  $H^l(q)$  in Eq 5 of the main text, are as follows. For acoustic phonons,  $H^l = H^l_{adp} + H^l_{pz}$ .  $H^l_{adp} = C^{0S}(z)$  from Eq (S5) using the strain phasors  $e_{ii}(z)$  from the acoustic mode of level l solved for in Sec S2) and the material dependent  $D_i(z)$  parameters.  $H^l_{pz} = -e\phi(z)$  where  $\phi$  is the piezoelectric potential generated by the acoustic mode of level l as solved in Sec S2.1). For polar optical phonons,  $H^l_{pop} = -e\phi(z)$  where  $\phi(z)$  is the potential coupled with the POP mode of level l. Finally, for the "generic extrinsic scatterer",  $H^l$  is just a constant (17.3 meV) tuned to fit the low-temperature mobility.

The transition rates are arranged to form a transition matrix  $R_{km}^{k'm'}$ , and thus Eq (4) of the main text is solved by a least squares procedure to find the perturbation-per-electric-field of the carrier distribution function, from which the mobility is extracted by an occupation-weighted sum of the group velocities.

#### References

- [1] Stefan Birner. "Modeling of semiconductor nanostructures and semiconductor electrolyte interfaces". PhD thesis. Technical University of Munich, 2011. ISBN: 9783941650350.
- [2] Cyrus E. Dreyer et al. "Correct implementation of polarization constants in wurtzite materials and impact on III-nitrides". In: *Phys. Rev. X* 6.2 (2016), p. 1. ISSN: 21603308. DOI: 10.1103/PhysRevX.6.021038.

- [3] M. J. Kane et al. "Determination of the dielectric constant of GaN in the kHz frequency range". In: Semiconductor Science and Technology 26.8 (2011), p. 1. ISSN: 02681242, DOI: 10.1088/0268/26/8/085006.
- [4] M. Kazan et al. "Directional dependence of AlN intrinsic complex dielectric function, optical phonon lifetimes, and decay channels measured by polarized infrared reflectivity". In: J. App. Phys. 106.2 (2009). ISSN: 00218979. DOI: 10.1063/1.3177323.
- [5] S. Komirenko et al. "Dispersion of polar optical phonons in wurtzite quantum wells". In: *Phys. Rev. B* 59.7 (1999), p. 5013. ISSN: 0163. DOI: 10.1103/PhysRevB.59.5013.
- [6] Evgenii P. Pokatilov, Denis L. Nika, and Alexander A. Balandin. "Confined electron-confined phonon scattering rates in wurtzite AlN/GaN/AlN heterostructures". In: J. App. Phys. 95.10 (2004), p. 5626. ISSN: 00218979. DOI: 10.1063/1.1710705.
- [7] Evghenii P. Pokatilov, Denis L. Nika, and Alexander A. Balandin. "Phonon spectrum and group velocities in AlN/GaN/AlN and related heterostructures". In: Superlattices and Microstructures 33.3 (2003), p. 155. ISSN: 07496036. DOI: 10.1016/S0749(03)00069.
- [8] G. B. Ren, Y. M. Liu, and P. Blood. "Valence-band structure of wurtzite GaN including the spin-orbit interaction". In: App. Phys. Letters 74.8 (1999), p. 1117. ISSN: 00036951. DOI: 10.1063/1.123461.
- [9] Patrick Rinke et al. "Consistent set of band parameters for the group-III nitrides AlN, GaN, and InN". In: Phys. Rev. B Condensed Matter and Materials Physics (2008). ISSN: 10980121. DOI: 10.1103/PhysRevB.77.075202.
- [10] I-H. Tan et al. "A self-consistent solution of Schrödinger-Poisson equations using a nonuniform mesh". In: J. App. Phys. 68.8 (Oct. 1990), p. 4071. ISSN: 00218979. DOI: 10.1063/1.346245.
- [11] I. Vurgaftman and J. R. Meyer. "Band parameters for nitrogen-containing semiconductors". In: J. App. Phys. 94.6 (2003), p. 3675. ISSN: 00218979. DOI: 10.1063/1.1600519.